Design and tool anchoring for a 120kN expander cycle rocket engine LOX turbopump

Louis Souverein, Chris Maeding, Thomas Aichner, Blazenko Ivancic, Adalbert Wagner and Manuel Frey
Airbus DS GmbH, 81633 Munich, Germany
Corresponding author: louis.souverein@airbus.com

Abstract

As part of a German nationally funded research programme "TARES", a turbopump initiative has been started in recent years within Airbus DS GmbH. The aim of this study is to design a liquid oxygen turbopump assembly (LOX-TPA) for a *120kN* thrust class expander cycle rocket engine. To realise this objective, Airbus DS GmbH builds on in-house heritage, notably the turbopumps of the P111 and the H20 staged combustion engines. This experience serves as input for the design of the *120kN* LOX turbopump. The current paper details the fluidic design of the turbopump, including the design philosophy and the anchoring on the heritage hardware. Discussed are the pump and turbine pre-design starting from the configuration trade-off, the preliminary design, the flow path and blade design, and the design of inlet/outlet and the volute. Finally, the performance (nominal and off-design) is characterised by means of 3D CFD simulations.

1. Introduction

In recent years, a turbopump initiative has been started Airbus DS GmbH as part of a German nationally funded research programme "TARES". The study is aimed at the design of a liquid oxygen turbopump assembly (LOX-TPA) for a *120kN* thrust class expander cycle rocket engine. In order to achieve this objective, a turbopump design process has been established, building on available software packages and capabilities with the acquisition of additional options and packages wherever necessary. For the anchoring of the design and simulation tools, Airbus DS GmbH draws on in-house heritage, notably the turbopumps of the P111 and the H20 staged combustion engines. Available design and test data have been used, with a focus on the redesign of the heritage hardware based on existing construction drawings and the original hardware itself. CFD simulation results of the P111 axial turbine were compared to available historic data in terms of performance, and studies have been initiated to re-characterise the H20 LOX inducer, both numerically and experimentally.

This experience serves as input for the design of the *120kN* LOX turbopump. A trade-off has been performed (see [1]) to define different configurations of the LOX-TPA, evaluating several alternatives to establish the most promising baseline design variant. Criteria include the pump and turbine efficiency, the cavitation margin, and the number of turbine stages. The selected baseline turbopump design consists of a high head inducer, radial impeller and vaned diffuser on the pump side driven by a single stage subsonic axial turbine on the same shaft.

The paper details the fluidic design of the turbopump, including the design philosophy and the anchoring on the heritage hardware. Discussed are, with the trade-off in [1] as starting point, the preliminary design based on 1D theory and semi-empirical correlations (inlet/outlet diameters, blade heights, number of blades, efficiency estimate, cavitation characteristics), the flow path and blade design (2D design of meridian contour, blade mean lines and blade profiling) and the design of inlet/outlet and volute. Finally, the performance (nominal and off-design) has been characterised by means of 3D CFD simulations, and the suction performance of the inducer is characterised experimentally.

2. Design process

As part of the "TARES" research program, one of the principal aims of the current initiative within Airbus DS GmbH has been to establish the turbopump design process for the development, see Figure 1, with the aim of developing a *120kN* LOX-turbopump. The design flow builds largely upon available software packages and capabilities. The design process has now been established by means of anchoring on available heritage hardware data and a full design loop for the *120kN* LOX-Turbopump including manufacturing and testing for the inducer hardware.

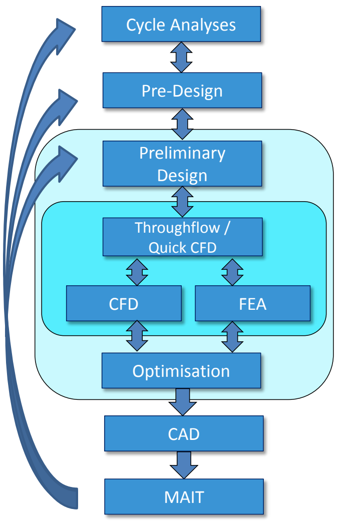

Figure 1: Established turbopump design flow

3. Anchoring on heritage data

In order to anchor the design process that has been established as part of the "TARES" research program, Airbus DS GmbH has drawn on its turbopump heritage. Most notably, the H20 *200kN* and the P111 *50kN* stage combustion engines have been used as validation cases, for which detailed design and test data are available (see [1]).

3.1 H20 LOX-Turbopump inducer

The first case for anchoring the design tools was the H20 LOX-inducer from the *200kN* H_2/O_2 staged combustion engine developed in Ottobrunn in the late 1960s and early 1970s for the Europa III rocket. Design and test reports are available from this period, documenting the thorough characterisations that were made on this inducer, including parameter studies concerning different geometrical properties. Tests were performed in both water and liquid oxygen (LOX) at rotational speeds between *20 000* and *40 000* rotations per minute (*rpm*), the latter being the nominal value for the LOX-pump. Table 1 shows the nominal inducer characteristics. The relevant quantities are defined in equation 1 (with the specific speeds being defined using the units *rpm*, m^3/s and *m* for respectively the rotational speed, the volumetric flow rate and the head). The original hardware is still available today and has recently been scanned as input for 3D-CFD simulations, see Figure 2. The existing hardware and design data have served as a basis for the current re-design of the inducer, see Figure 3. In addition to an anchoring of the design tool, it can serves as a basis for further CFD investigations, in particular for cavitation modelling studies. These are currently being undertaken by the DLR Göttingen in the context of the Propulsion2020 cooperation. In addition, the original inducer hardware will be re-characterised in an upcoming test campaign at the University of Kaiserslautern.

$$Nss = \frac{N\sqrt{Q}}{NPSHR^{0.75}} \qquad Ns = \frac{N\sqrt{Q}}{(\Delta H)^{0.75}} \qquad \Phi = \frac{C_m}{U} \qquad \Psi = \frac{2\Delta P}{\rho U^2} \tag{1}$$

Figure 2: H20 LOX inducer: original test hardware (respectively Inconel and Aluminum) (left) and 3D-scan (right)

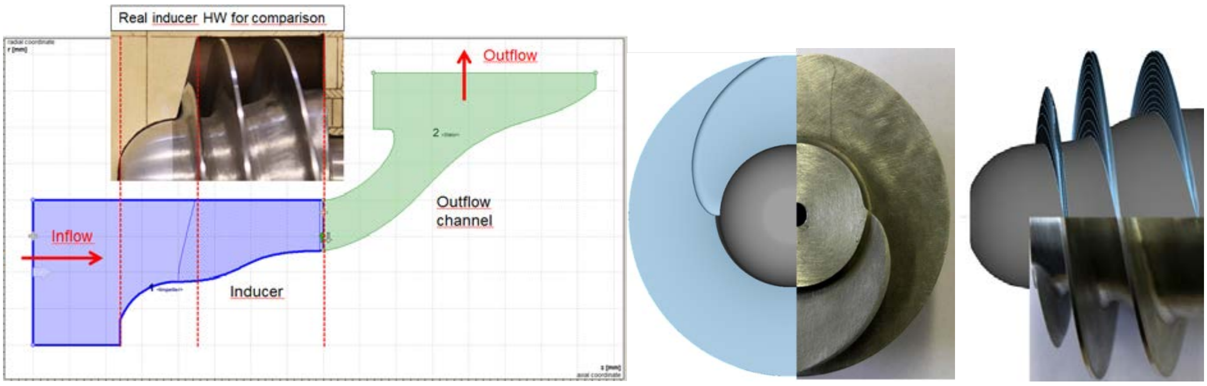

Figure 3: H20 LOX inducer: redesign of original hardware for CFD-validation

Table 1: Original test data for the H20 inconel LOX inducer

Original hardware: Nominal inducer characteristics		
Quantity		
Fluid		LOX
Rotation rate	N (rpm)	40000
Flow coefficient, inlet	$\Phi_{ind,in}$ (-)	0.067
Head coefficient	Ψ_{ind} (-)	0.075
Suction specific speed	Nss	886
Net positive suction pressure required	NPSPR (bar)	2.2

3.2 P111 axial turbine

The P111 LOX/kerosene *50kN* staged combustion engine, developed in the 1960s in Ottobrunn, was chosen as the second anchoring case for the design tools. In particular the single stage reaction turbine, driven by an oxygen rich preburner, was a valuable validation case. The original hardware, including design and test documentation, is available and has served as input for the redesign and the 3D CFD simulations.

The original P111 power-pack hardware, an excerpt of the construction drawing of the axial turbine and the blade profiles are shown in Figure 4. The figure also shows (at the bottom right) the numerical mesh used for the 3D CFD simulations of the redesign of the P111 axial turbines. The computational grid has a total size of ca. *1.4 million* cells. It is divided into two domains: the stator domain with *500 000* cells and the rotor domain with *900 000* cells, both resolving a single blade. The resolution, especially at the wall, is sufficient to capture all relevant flow phenomena in the simulation. The appropriate periodic boundary conditions were used to represent the complete turbine behaviour.

The CFD results are shown in Figure 5, with the left side depicting the static pressure field normalised by the total inlet pressure and the right side displaying the relative Mach field. Shown are for both fields a blade-to-blade view generated at a relative blade span of *0.5* (top figure) and a mass weighted meridional view.

The performance results from the 3D-CFD simulation are compared to the heritage hardware data in Table 2. The original efficiency has been determined from the test data. To enable a proper comparison with the current simulation results, the mechanical losses and the disk friction losses have been corrected for in the heritage data based on the original design estimates for these loss contributions. A good agreement between the original data and the simulation results has been obtained. Additionally, the comparison has provided important information on the different factors influencing the turbine performance, as well as the breakdown of the loss contributions.

Table 2: P111 axial turbine characteristics compared with CFD results

Original hardware: Nominal characteristics		
Quantity	Parameter	Value
Rotation rate	N (rpm)	25800
Isentropic velocity ratio	U/C_0 (-)	0.5
Reaction rate	ρ (-)	0.237
Total-to-static pressure ratio	π_{ts} (-)	1.39
Total-to-static efficiency	η_{TS} (-)	0.79
CFD results: Nominal characteristics		
Quantity	Parameter	Value
Total-to-static pressure ratio	π_{ts} (-)	1.45
Total-to-static efficiency	η_{TS} (-)	0.77

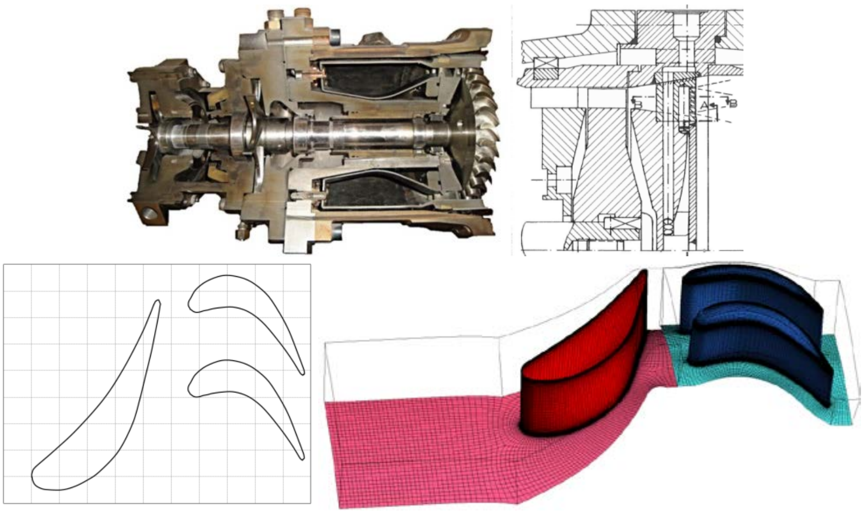

Figure 4: P111 original and re-designed (CFD-mesh) axial turbine geometry

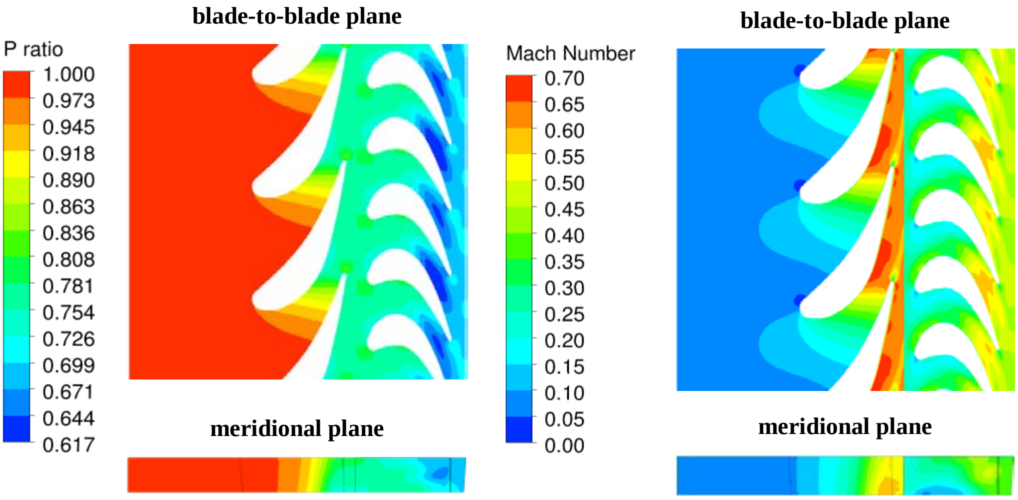

Figure 5: 3D-CFD results for the P111 axial turbine. Left: pressure ratio ($p_{stat}/p_{tot,in}$); right: relative Mach number

4. 120kN Turbopump design

The re-design experience, consecutive tool anchoring activities and the planned test campaign with the heritage hardware all serve to establish the work flow for the Airbus DS GmbH turbopump design activities. This section details the current flow path design of the *120kN* turbopump that shall establish a baseline for further optimisation studies.

4.1 Design requirements and configuration trade-off

Based on the operating requirements (see Table 3 for the nominal conditions) for the *120kN* turbopump, a dedicated trade-off has been performed (for details see [1]) to define different configurations of the *120kN* LOX-TPA, evaluating several alternatives to identify the most promising design variants. The selected baseline turbopump configuration consists of a radial diffuser pump with a high head inducer driven by a single stage subsonic axial turbine on the same shaft with a rotational speed of *25 000* rotations per minute (*rpm*).

4.2 Pump fluid path design

Based on the nominal pump requirements and the selected rotational speed of *25 000 rpm*, a preliminary sizing was performed. The relevant non-dimensional parameters are defined in Eq.1 above. A first pump diameter and efficiency estimate was made based on the *Ns-Ds*-diagram, see [2]. In addition, an estimate of the minimum required shaft diameter was made. The number of blades $Z=6$ was based on the correlations from [3] and [4]. The suction characteristics of a pump stage without inducer were evaluated based on the Pfleiderer criterion (see [4]). This yields a first estimate of the net positive suction head required (*NPSHR*), confirming indeed the need for an inducer. These estimates give a first idea of the overall dimensions of the pump, and the requirements in terms of suction specific speed and inducer head.

Based on these pre-design estimates, a preliminary design of the inducer was made. The inducer inlet was sized based on the Brumfield criterion to attain a minimal *NPSHR* value that provides sufficient cavitation margin. Following the approach from [5], an optimal flow coefficient of $\Phi_{ind,in}=0.1$ was selected, in line with values for other realized LOX-inducers, see [2]. This is conservative in terms of the attained minimum experimental values specified in [5]. The inducer inlet hub-to-shroud ratio was determined based on a geometrical comparison with existing inducers (amongst others the H20-LOX inducer). The outlet hub-to-shroud ratio and the outlet angle were determine based on a parametric study, requiring that *NPSHA>NPSHR* at the impeller inlet with a margin that was anchored on existing hardware. As a baseline, the inducer outlet diameters at the hub and shroud and the impeller inlet diameters were fixed to the same value, verifying that the impeller suction diameter was close to the ideal value in terms of *NPSHR*. The blade number was set to $Z=3$ and the solidity were selected based on the recommendations from [5]. A sweep angle was selected for increased suction performance and to decrease the bending load on the 'corner flap' of the blade leading edge. The value for the tip clearance was based on H20 experience.

The shrouded impeller was designed to attain the required total head rise at a nominal head coefficient value of $\Psi_{imp}=0.85$ using semi-empirical design functions and simultaneous anchoring on available reference data for existing pumps. The outlet blade height to impeller diameter ratio was set to yield a meridional deceleration close to unity. The axial extension of the impeller was sized according to Gülich, see [6]. The outlet angle was set in agreement with the recommendation from [3]. The blade mean lines were chosen such as to obtain a monotonous static pressure rise, while satisfying the Ackeret criterion for the relative velocity. The wrap angle was set to the maximum value that still enables manufacturing by means of milling.

Table 3: *120kN* turbopump: required characteristics

120kN Turbopump nominal operating conditions		
Pump requirements		
fluid	LOX	-
nominal flow rate (at the outlet)	22.8	kg/s
total pressure at the pump inlet	3	bar
pump inlet temperature	91.5	K
pump outlet total pressure	81.8	bar
Turbine requirements		
fluid	H2	-
mass flow rate (incl. LOX TP bypass)	2.67	kg/s
bypass mass flow rate	>20	%
total pressure at the inlet	89	bar
inlet temperature	218	K
static pressure at the outlet	75	bar

Table 4: Pump design overview

Nominal pump characteristics		
Quantity	Parameter	Value
Rotation rate	N (rpm)	25000
Specific speed (SI)	Ns (-)	25.9
Design flow coefficient	Φ_{pump} (-)	0.09
Design head coefficient	Ψ_{pump} (-)	0.95
Net positive suction head available	NPRHA (m)	17.0
Hydraulic efficiency	η_{hyd} (-)	0.80
Pump overall efficiency	η_{tot} (-)	0.68
Shaft power	P_{shaft} (kW)	-236
Nominal inducer characteristics		
Quantity	Parameter	Value
Design flow coefficient, inlet	$\Phi_{ind,in}$ (-)	0.10
Design head coefficient	Ψ_{ind} (-)	0.22
Design suction specific speed	Nss (-)	689
Net positive suction head required	NPSHR (m)	9.6
Number of inducer blades	Z_{ind} (-)	3
Solidity	σ (-)	2.8
Hub/shroud ratio, inlet	Dh_1/Ds_1	0.4
Hub/shroud ratio, outlet	Dh_2/Ds_2	0.6
Nominal main impeller + diffusor characteristics		
Quantity	Parameter	Value
Design head coefficient	Ψ_{imp} (-)	0.85
Number of impeller blades	Z_{imp} (-)	6
Suction diameter/imp. diameter	Ds_1/D_2	0.7
Number of diffusor blades	Z_{diff} (-)	10
Diffusor outlet diameter/imp. diameter	D_4/D_2	1.30

The vaned diffuser was designed following recommendations from [3],[7],[8] and [9] for the geometrical sizing of diameters, gaps and clearances. The number of diffuser vanes was taken equal to the optimum value based on considerations of periodicity to avoid interaction with the impeller blades. The volute was designed for the maximum expected off-design flow with a circular cross-section, folded inwards for compactness and flow stability. The cross-sectional area was determined using the Pfleiderer approach, see [4].
The resulting geometrical design and the design estimates for the nominal total and static pressure and the absolute velocity progressions through the pump are shown in Figure 6. The overall pump design is summarized in Table 4.

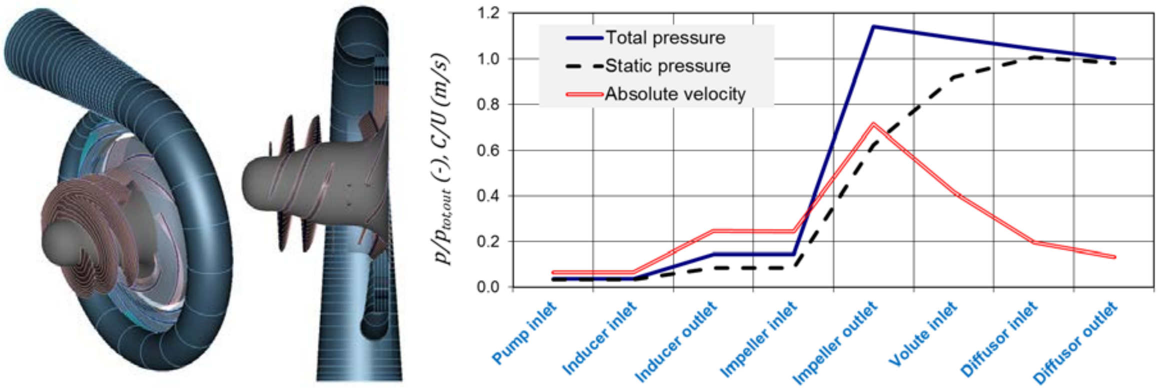

Figure 6: *120kN* LOX-pump design (left), estimated nominal progression of pressure and absolute velocity (right)

A 3D CFD-analysis was made as basis for further optimization loops. The computational grid encompasses the full 360° pump geometry and contains a total of ca. *5.8* million cells divided over 4 domains: *1.7* million for the inducer, *1.6* million for the impeller, *2.2* million for the diffuser and *350 000* for the volute. The resolution, especially at the wall, is sufficient to capture all relevant flow phenomena in the simulation. Figure 7 shows the CFD result for the static pressure fields normalized by the total outlet pressure. The particle traces (coloured by the absolute velocity) are visualized in Figure 8 for several flow coefficient values. The figure also shows the obtained off-design performance computed for several operating points, including a polynomial fit. The flow visualisations for the lower operating points show clear signs of flow break down, which is reflected in the efficiency. The nominal operating point shows a regular flow behavior through the pump with a single vortex in the volute and the presence of a tip vortex at the inducer inlet, as has been explained by [10]. For flow rates superior to the foreseen application range, the inducer inlet tip vortex disappears whereas elevated velocities start to occur within the volute (as is to be expected since it operates outside its design range). The flow coefficient varies within approx. *±10%* from the nominal value for the foreseen operating envelope, which is where the maximum efficiency is obtained. The CFD predictions indicate a *5%* higher hydraulic efficiency for the whole pump design than estimated in the preliminary design. The current design and simulation results provide the baseline for developing a physical understanding of the relevant flow phenomena as input for further optimization studies.

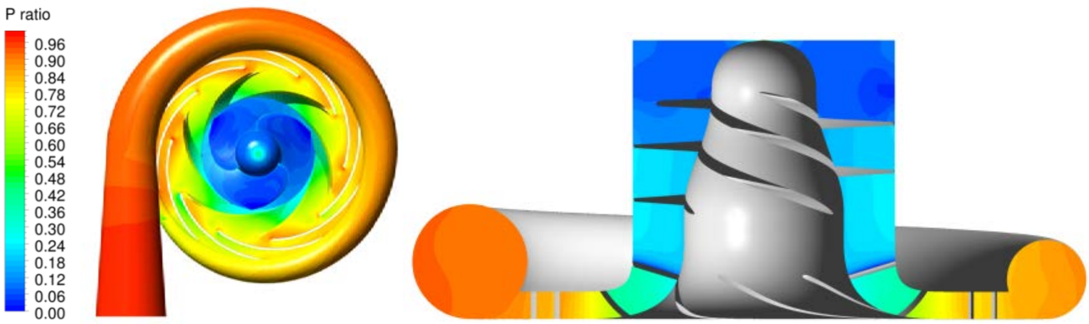

Figure 7: *120kN* LOX-pump nominal pressure iso-contours ($p_{stat}/p_{tot,out}$)

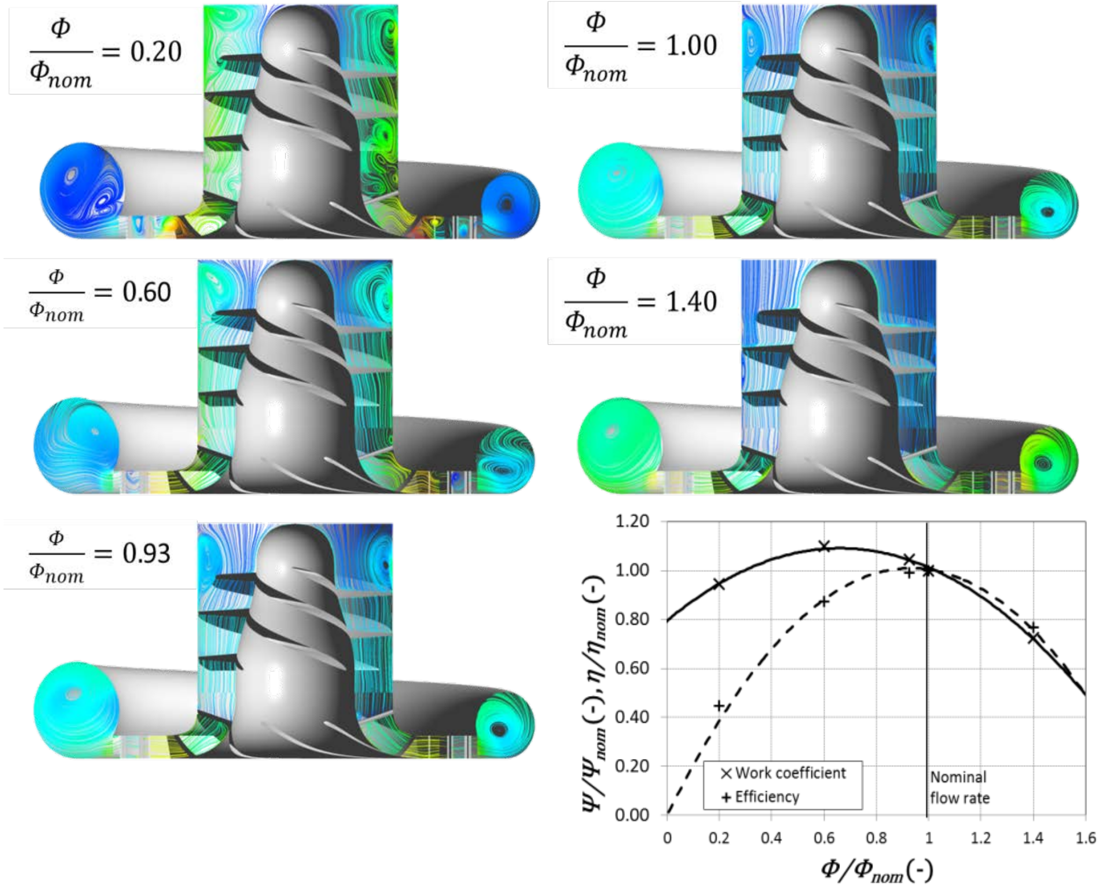

Figure 8: *120kN* LOX-pump off design predictions

4.3 Axial turbine flow path design

The trade-off in [1] has identified a single stage impulse turbine (reaction rate $\rho<0.15$) as a viable option to produce the required shaft power for driving the LOX-pump while complying with the nominal operating conditions specified in Table 3. To start the design process, the turbine efficiency is a necessary input which determines in particular the rotor diameter and the combination of stator exit angle and blade height. The nominal characteristics in Table 3 with a *20%* bypass mass flow rate directly prescribe a minimum overall efficiency level of $\eta=68\%$ to attain the necessary power output; this is achievable based on the existing hardware values presented in [2].

The isentropic velocity ratio U/C_0 is taken as the governing parameter for the turbine efficiency, with the spouting velocity C_0 resulting from the input parameters. To make a detailed trade between efficiency η_{TS}, stator exit angle α_1, turbine disk diameter D_m and rotor blade height b_r, the relation from [12] was evaluated in detail. Considering only the stator exit angles yielding the maximum efficiency (i.e. $10°<\alpha_1<15°$, defining all angles relative to the circumferential direction), the relation agrees well with the other theoretical and empirical relations that were considered (refs. [3],[11],[12],[13],[14],[15]). All curves attain a maximum efficiency η_{TS} between *79%* and *84%* with the optimal U/C_0 in the range of *0.40-0.55*, see Figure 9, providing an indication of the required U/C_0.

The efficiency estimates for the current design case based on the correlation from [12] are shown in Figure 10. The interdependence of the isentropic velocity ratio, the stator exit angle and the rotor diameter and blade height is also shown. A stator exit angle of $\alpha_1=80°$ at $U/C_0=0.4$ seems to offer the best compromise between efficiency and blade height for the first design, yielding a predicted efficiency of $\eta_{TS}=81\%$. This is sufficient for attaining an overall efficiency of $\eta=68\%$ based on the P111 heritage data, noting that the maximum for the total-to-total efficiency is very flat and the optimum efficiency value is also obtained close to $U/C_0=0.4$. Smaller values of U/C_0 would reduce the efficiency and hence potentially compromise the bypass mass flow rate requirement, and larger values of α_1 would progressively reduce the blade height, leading to unrealizably small blades. The basic blade height was taken constant for the whole length of the turbine (stator inlet, rotor inlet/outlet), with only a slight contraction at the stator outlet based on recommendations from [15].

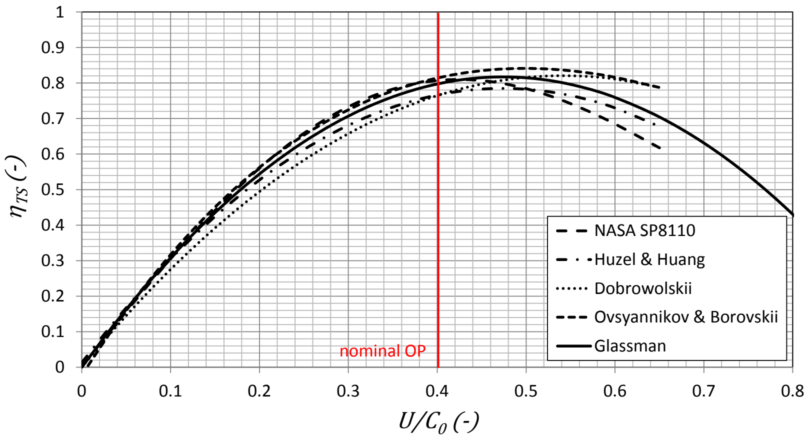

Figure 9: Total-to-static efficiency estimate correlations from literature

Based on this preliminary sizing, and providing the reaction rate of $\rho=0.15$ selected in the trade-off (see [1]), the velocity triangles now follow directly from the 1D design. Using flow deviation values for the fluid leaving the stator blades based on [15], the required blade angles were estimated. The blade length was calculated based on empirical correlations and a comparison to existing hardware. Finally, the blade design was generated starting from available standard profiles, using the respective recommended values for pitch and stagger angle for the selected profiles. The final blade profile was generated by means of Bezier curves, using optimization loops with CFD predictions to attain the desired hydraulic power output of the turbine. The overall axial turbine design is summarized in Table 5. The blade and meridional design are shown in Figure 11, together with the velocity triangles (values are normalized by the blade speed *U*) and the progression of the flow quantities through the turbine (the stations represent the stator inlet (0), stator outlet/rotor inlet (1) and rotor outlet (2) respectively).

In view of the inlet and outlet design for the turbine, a trade was made with respect to the flow direction. A configuration with inlet manifold and axial outlet was compared with a configuration with axial inlet and outlet volute. The latter configuration has been selected as baseline as it is expected to be the most favourable in terms of axial thrust balancing, it provides an axial inflow to the turbine stator, and it has the potential of minimising losses at the turbine outlet by reabsorption of the residual swirl component.

Table 5 : Axial turbine design overview

Nominal turbine characteristics		
Quantity	Parameter	Value
Rotation rate	N (rpm)	25000
Isentropic velocity ratio	U/C_0 (-)	0.4
Total-to-static pressure ratio	π_{ts} (-)	1.19
Bypass mass flow rate percentage	(%)	20
Reaction rate	ρ (-)	0.15
Total-to-static efficiency	η_{TS} (-)	0.81
Overall efficiency (min. value)	η (-)	0.68
Shaft power	P_{shaft} (kW)	236
Stator main dimensions		
Quantity	Parameter	Value
Hub-to-shroud ratio	D_h/D_s (-)	0.936
Inlet flow angle (absolute)	α_0 (deg)	90
Outlet flow angle (absolute)	α_1 (deg)	10
Stagger angle	γ_s (deg)	30
Number of blades	Z_s (-)	30
Rotor main dimensions		
Quantity	Parameter	Value
Hub-to-shroud ratio	D_h/D_s (-)	0.933
Inlet flow angle (relative)	β_1 (deg)	20
Outlet flow angle (relative)	β_2 (deg)	16
Stagger angle	γ_r (deg)	80
Number of blades	Z_r (-)	65

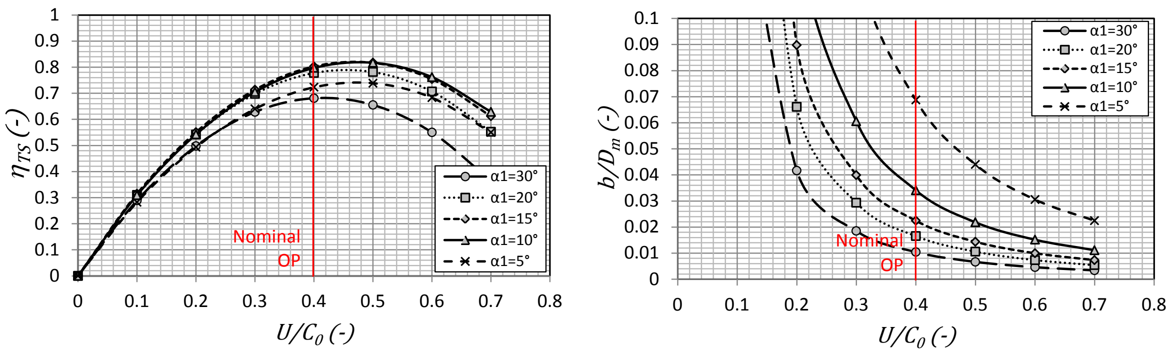

Figure 10: Optimisation results for efficiency, rotor diameter and blade height

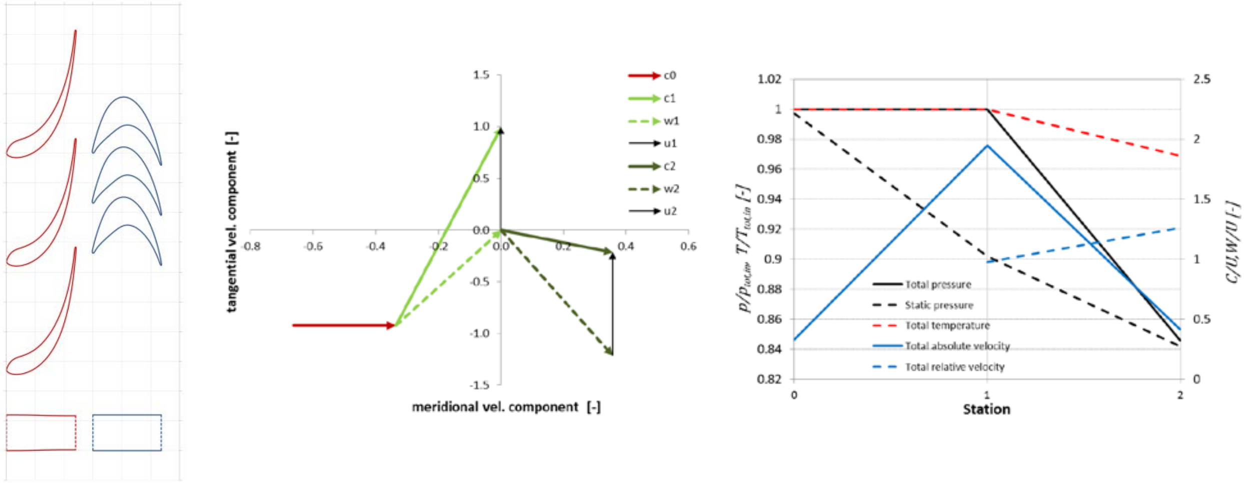

Figure 11: Blade and meridional design (left), velocity triangles normalized by the rotor speed *U* (middle) and normalized flow quantities progression (right)

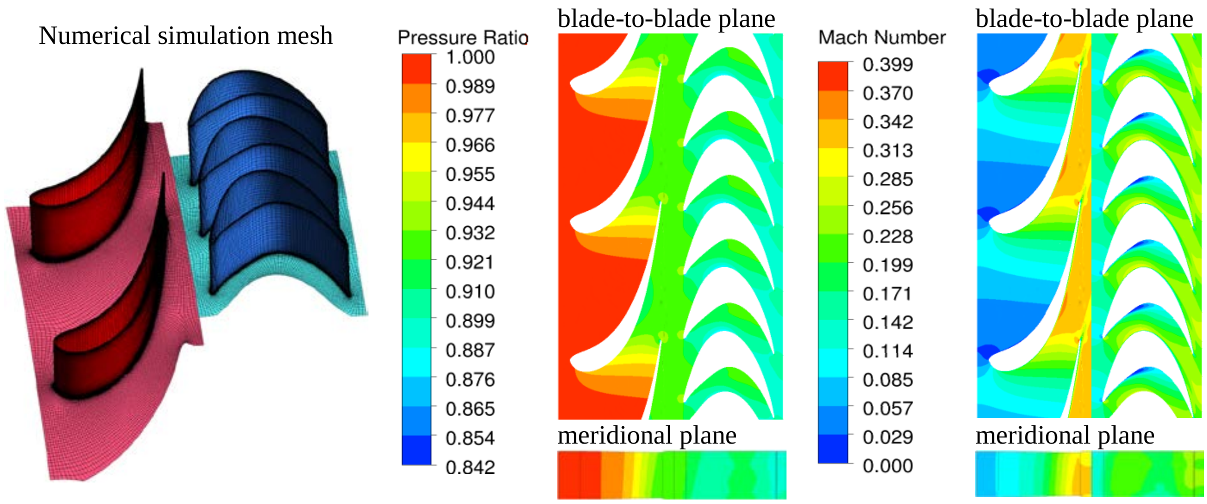

Figure 12: 3D-CFD results for the *120kN* axial turbine. Left: numerical mesh; middle: pressure ratio ($p_{stat}/p_{tot,in}$); right: relative Mach number

Figure 12 shows the geometry with the applied numerical mesh for the 3D CFD simulations as well as representative results of these turbine simulations. The computational grid has a total size of ca. *1.3 million* cells. It is divided into two domains: the stator domain with *1.0 million* cells and the rotor domain with *300 000* cells, both resolving a single blade. The resolution, especially at the wall, is sufficient to capture all relevant flow phenomena in the simulation. The appropriate periodic boundary conditions were used to represent the complete turbine behaviour. Concerning the CFD results in Figure 12, the middle pane depicts the static pressure field normalised by the total inlet pressure and the right pane displays the relative Mach field. Shown are for both fields a blade-to-blade view generated at a relative blade span of *0.5* (top figure) and a mass weighted meridional view. The current design and simulation results provide the baseline for developing a physical understanding of the flow phenomena as input for further optimization studies. For example, a more homogeneous blade-to-blade Mach distribution through the rotor blade channel would be desirable, as low relative velocities are observed locally on the concave side of the rotor blade. However, the desired efficiency of $\eta_{TS}=81\%$ has already been attained with the current design. Further parametric studies will be performed to optimise the turbine fluid flow path in order to maximise the performance.
To summarize the fluidic design, Figure 13 shows the 3D-CAD view of the rotating parts of the *120kN* turbopump design including all principal fluidic parts (inlets/outlets, volutes, diffusers).

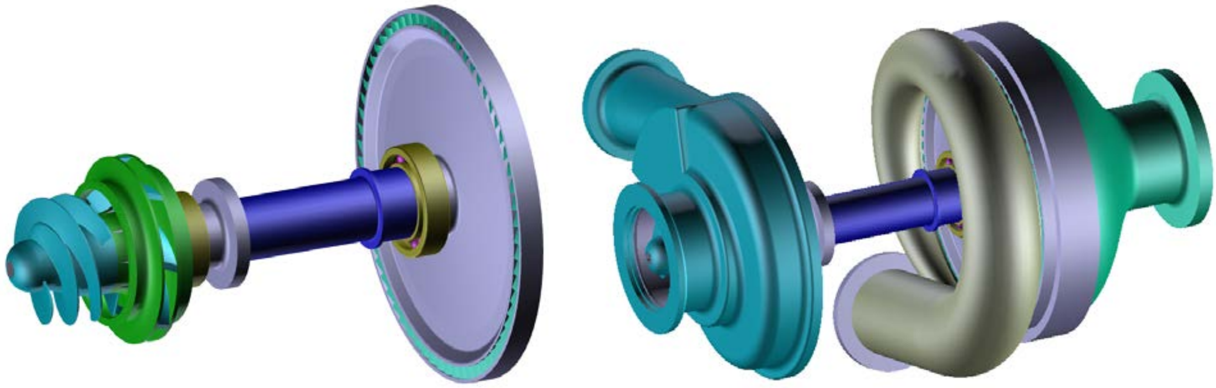

Figure 13: 3D CAD-view of the *120kN* turbopump design: rotating parts (left) and flow path including in/outlets (right)

5. 120kN test activities

Inducer characterisation tests in water are currently ongoing at the Von Karman Institute of Fluid Dynamics (VKI) in the frame of an Airbus DS funded activity. The scaling to attain the proper test conditions is shown in Table 6. The inducer has geometrically been scaled-up to fit the test section and manufactured from a polymeric material (ABS) by means of rapid prototyping, see Figure 14. The hub contour has been extended to accommodate the larger test bench interface diameter. The rotation speed and flow rate have been scaled based on flow coefficient and head coefficient similarity, verifying that the Reynolds number is sufficiently high to attain similarity of the inducer performance. In addition, the water is heated to the appropriate temperature to attain thermal similarity with liquid oxygen based on the thermal effect parameter Σ^*, see [8]. The tests will be evaluated to confirm the inducer characteristics, both in terms of achieved head coefficient and attained suction performance. In addition, the dynamic cavitation behaviour will be characterised. The first cavitation visualisation results are shown in Figure 15, starting from the nominal conditions on the left down to a cavitation coefficient of $\sigma=0.25$ on the right. The first occurrence of cavitation is highlighted by the red ellipse. The test campaign results shall serve as input for the validation of the design tools, the CFD-simulations and cavitation models as baseline for further inducer optimisations.

Table 6: Scaling for water tests

Inducer scaling: LOX operating conditions to water test conditions		
Quantity	LOX	Water
Inlet temperature, T_{in} (K)	91.5	338.7
Rotation rate, N (rpm)	25000	1500
Geometrical scale (-)	1:1	1.3:1
Flow coefficient, $\Phi_{ind,in}$ (-)	0.10	0.10
Head coefficient, Ψ_{ind} (-)	0.22	0.22
Thermal effect parameter, Σ^*(-)	73.6	73.6
Net positive suction head required, NPSHR (m)	9.6	0.054
Suction specific speed, Nss	689	689

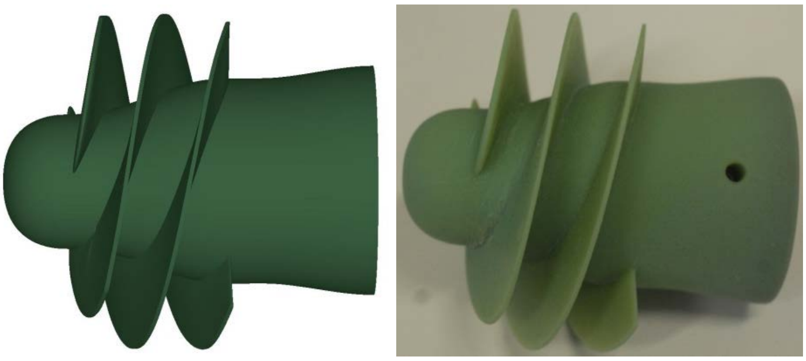

Figure 14: *120kN* LOX-inducer design (left) compared to rapid prototyping test hardware (right)

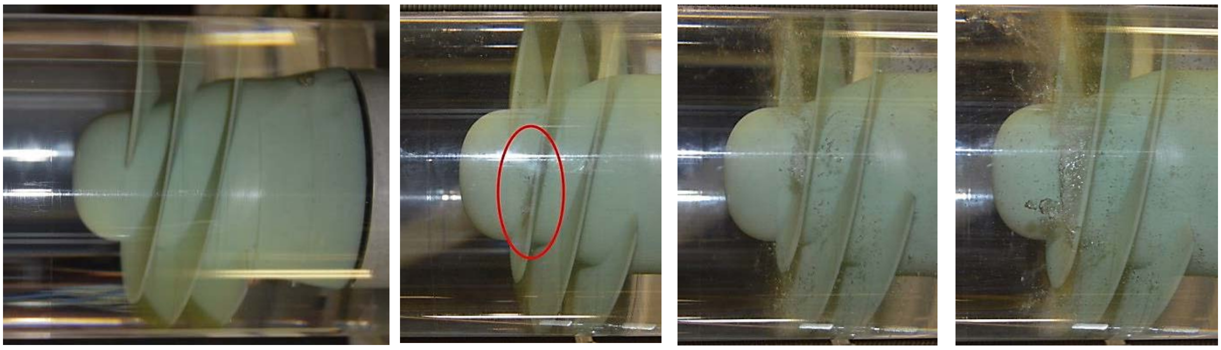

Figure 15: *120kN* LOX-inducer during cavitation testing at the VKI

6. Conclusions

Within the context of the German nationally funded research programme "TARES", several activities have been initiated to build-up and re-establish turbopump design competences within Airbus DS GmbH. The main focus has firstly been on the anchoring of the fluidic design and simulation tools on in-house heritage hardware; subsequently a design was made of a liquid oxygen (LOX) turbopump for a *120kN* thrust class expander cycle rocket engine, including accompanying experimental and modelling efforts. These activities have served to attain the following milestones:

- Re-establishing proven design heritage based on the H20 *200kN* and the P111 *50kN* staged combustion engine turbopump hardware
- Anchoring of the turbopump fluidic design tools to the heritage hardware and available literature data for existing turbopumps
- Generating a *120kN* LOX-turbopump design including all main flow path components
- Performing 3D-CFD simulations of the heritage hardware and the *120kN* turbopump design
- Obtaining first cavitation test results in water of the *120kN* LOX-inducer design

Further activities are still in progress and upcoming, such as the hydraulic characterisation campaigns for the *120kN* LOX-inducer and the heritage H20 LOX-inducer. The results of these campaigns will deliver validation data for 3D-CFD simulations and cavitation modelling.
These milestones serve to establish the Airbus DS GmbH fluidic design process and have provided a baseline turbopump design for further optimisations, experimental investigations and modelling studies.

Acknowledgements

This work was performed within the national technology program TARES. This program is sponsored by the German Space Agency, DLR Bonn, under contract No. 50RL1210. This support is gratefully acknowledged here. In addition, the effective cooperation with the Von Karman Institute for Fluid Dynamics (VKI) is gratefully acknowledged.

References

[1] Maeding, C., Souverein, L., Hummel, D., Koenigbauer, S., Wagner, A., Alting, J. 2015. A Preliminary Design Study for an Expander LOX Turbopump. In: *Proceedings of the 6th European Conference for Aeronautics and Space Sciences*, Krakow, Poland.

[2] Schmidt, G. 1999. Technik der Flüssigkeits-Raketentriebwerke. DaimlerChrysler Aerospace.

[3] Huzel, D.K., and Huang, D.H. 1992. Design of Liquid-Propellant Rocket Engines. In: *AIAA Progress in Aeronautics*. Vol.147, Washington DC, USA.

[4] Pfleiderer, C. 1955. Die Kreiselpumpen für Flüssigkeiten und Gase. 4th Ed., Springer.

[5] Jakobsen, R.B. 1971. Liquid Rocket Engine Turbopump Inducers. NASA SP8052.

[6] Gülich, J.F. 2010. Kreiselpumpen–Handbuch für Entwicklung, Anlagenplanung und Betrieb. 3rd Ed., Springer.

[7] Furst, J.K. 1973. Liquid Rocket Engine Centrifugal Flow Turbopumps. NASA SP8109.

[8] Brennen, C.E. 1994. Hydrodynamics of Pumps. Concepts ETI, Inc., Vermont, USA.

[9] Guinzburg, A., Williams, M., and Ferguson, T. 2002. Deep Throttle Turbopump Technology Design Concepts, JANNAF, April 8-12, 2002, Destin, Florida, USA.

[10] Arnone, A, Boncinelli, P., Munari, A., Spano, E. 1999. Application of CFD techniques to the design of the Ariane 5 turbopump. AIAA-99-3380.

[11] Glassman, A.J. 1994. Turbine Design and Application. NASA SP-290.

[12] Glassman, A.J. 1992. Computer Code for Preliminary Sizing Analysis of Axial-Flow Turbines. NASA CR-4430.

[13] Ovsyannikov, B.V., and B. I. Borovskii, B.I. 1971. Theory and analysis of the power-supply units of the liquid fuel rocket engines. Mashinostroyenie, Moscow (in Russian).

[14] Dobrovolskii, M.V. 1968. Liquid Fuel Rocket Engines. Mashinostroyenie, Moscow (in Russian).

[15] Douglas, H.W. 1974. Liquid rocket engine turbines. NASA SP-8110